

## Unipolar to Ambipolar Semiconductivity Switching in Charge Transfer Cocrystals of 2,7-di-*tert*-Butylpyrene

Arkalekha Mandal,<sup>a\*</sup> Pravasini Swain,<sup>b‡</sup> Bhaskar Nath,<sup>c‡</sup> Sudip Sau,<sup>a</sup> Prasenjit Mal<sup>a\*</sup>

<sup>a</sup>School of Chemical Sciences, National Institute of Science Education and Research (NISER)

<sup>b</sup>School of Physical Sciences, National Institute of Science Education and Research (NISER), HBNI, Bhubaneswar, PO Bhimpur-Padanpur, District Khurda, Odisha 752050, India

<sup>c</sup>Department of Educational Science, Assam Central University, Silchar, India, 788011

<sup>‡</sup> Authors have equal contribution

E-mail: [arkalekha@niser.ac.in](mailto:arkalekha@niser.ac.in)

### EXPERIMENTAL SECTION

#### Syntheses of Co-crystals 1-3

**Synthesis of co-crystal 1 (CCDC 1840880).** Equimolar amounts of 2,7-di-*tert*-butylpyrene (63 mg, 0.2 mmol) and TCNQ (40 mg, 0.2 mmol) were grinded with the assistance of 0.5 w% of toluene for 1 h. The resulting bluish green solid was dissolved in toluene to produce needle shaped blue crystals after a week.

**Synthesis of co-crystal 2 (CCDC 1840881).** Equimolar amounts of 2,7-di-*tert*-butylpyrene (63 mg, 0.2 mmol) and tetracyanobenzene (36 mg, 0.2 mmol) were suspended in CHCl<sub>3</sub> and

stirred for 30 min to produce crimson powder. Crystals suitable for X-ray study were grown by slow evaporation of THF solution in three days.

**Synthesis of co-crystal 3 (CCDC 1840882).** Equimolar amounts of 2,7-di-*tert*-butylpyrene (63 mg, 0.2 mmol) and 1,3-dinitrobenzene (33 mg, 0.2 mmol) were grinded with the assistance of 0.5 w% of methanol for 1 h. The resulting yellow solid was dissolved in CHCl<sub>3</sub>/Hexane (1:2) to produce block shaped crystals in two days.

**Characterization.** The co-crystals were characterized by single crystal X-ray, powder X-ray diffraction analyses as well as UV-Vis absorption and FT-IR spectra of the powdered samples. Optical band gap was calculated from UV-Vis spectra following the Kubelka-Munk equation  $E = hc/\lambda$ , where  $h$  denotes Plank constant. SEM images of the crystals were taken for studying morphology.

**Crystal Structure Refinement and Analyses.** The crystal structures were refined by direct method using SHEXL-14. All non-hydrogen atoms were refined anisotropically. Hydrogen atoms were derived from FMAP and further refined isotropically. The parameters of intermolecular interactions were derived using PARST programme implemented in PLATON and the crystal packing diagrams were obtained by Mercury 3.9.

**Theoretical Calculations.** All theoretical calculations were performed on crystal co-ordinates as the starting geometry using Gaussian09 programme package. The adiabatic ionization potential and electron affinities were calculated taking optimized geometries of the radical cation and anions in consideration. The HOMO, LUMO energies and static dipole moment (SDM) were calculated on crystal geometry of the co-crystals employing DFT calculations at M06-2X/6-311+G(d,p) level of theory to take account of the dispersive nature

of  $\pi\cdot\pi$  stacking.<sup>1</sup> The charge transfer integrals were calculated using orbital energies of dimers and trimers obtained from crystal geometries. Coulomb attenuated version of B3LYP (CAM-B3LYP) functional and 6-311G(d,p) basis set were used for accounting long range correction (LRC).<sup>2</sup> Wavelength, oscillator strength and orbital contributions for vertical excitation were calculated by TD-DFT method using CAM-B3LYP/6-311G(d,p) level of theory on crystal geometries of **1-3**. The interaction energy of dimeric D–A pairs were calculated at M06-2X/6-311G(d,p) level of theory following basis set superposition error corrected (BSSE) method of Boys and Bernardi.<sup>3</sup>

**Device Fabrication.** The Si/SiO<sub>2</sub> surface was cleaned successively with acetone and isopropanol. A small portion of the surface was chemically etched by HF solution to remove the oxide layer and make the gate electrode. The single crystal was subsequently placed along the long crystal axis on Si/SiO<sub>2</sub> surface. The source and the drain electrodes were prepared from two sides of the single crystal and the gate electrode was prepared from the HF etched portion by using Ag conductive paste.

## References

1. Y. Zhao, D. G. Truhlar, *Theor. Chem. Acc.*, 2007, **120**, 215.
2. A. Pedone, *J. Chem. Theory Comput.*, 2013, **9**, 4087.
3. S. F. Boys, F. Bernardi, *Mol. Phys.*, 1970, **19**, 553.

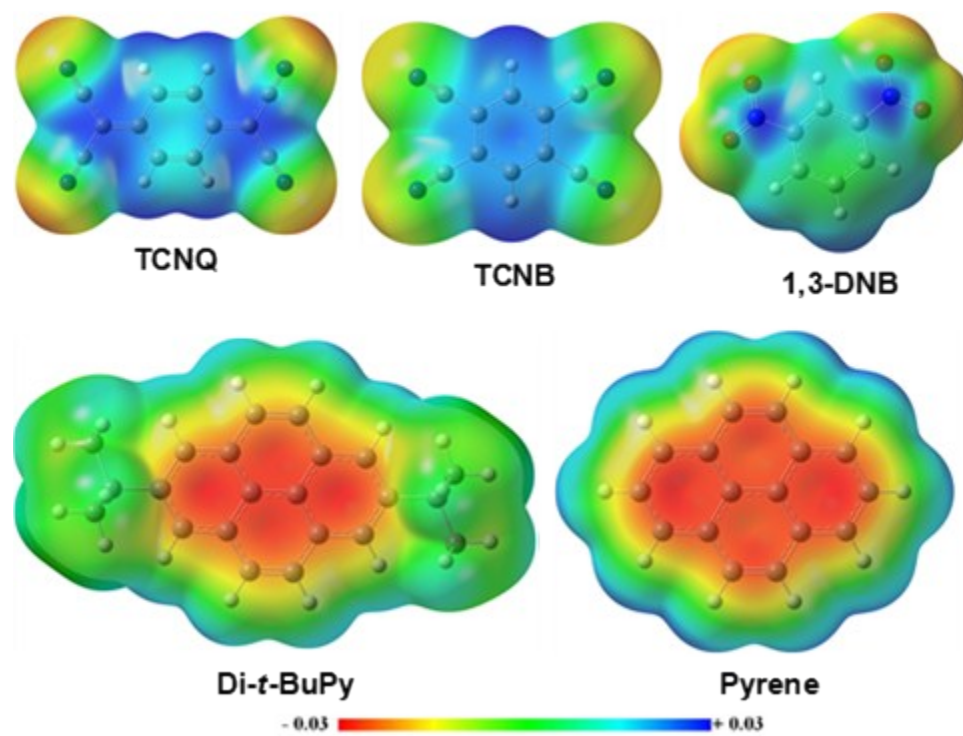


**Figure S1.** MEP diagrams of donor di-*t*-BuPy and acceptors TCNQ, TCNB and 1,3-DNB; MEP of pyrene is shown for comparison.

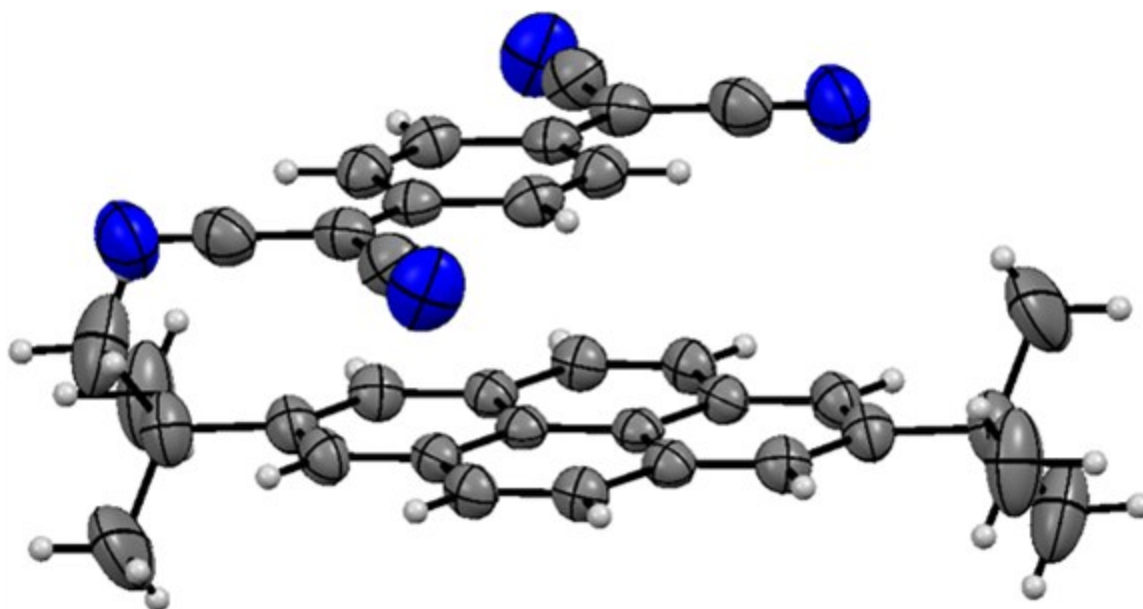


**Figure S2.** ORTEP diagram of cocrystal 1.

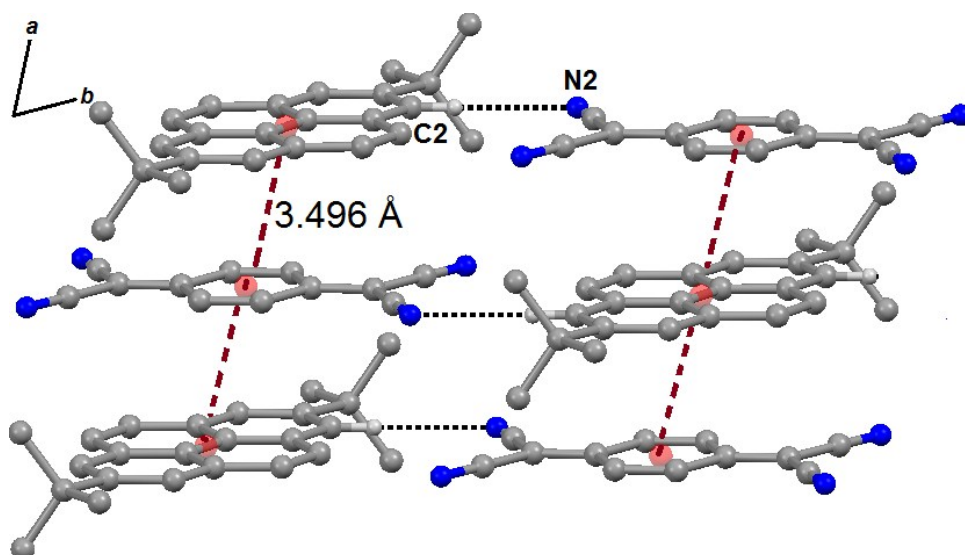


**Figure S3.** Crystal packing of cocystal 1 is stabilized by face to face  $\pi$ ··· $\pi$  stacking and C–H···N hydrogen bond.

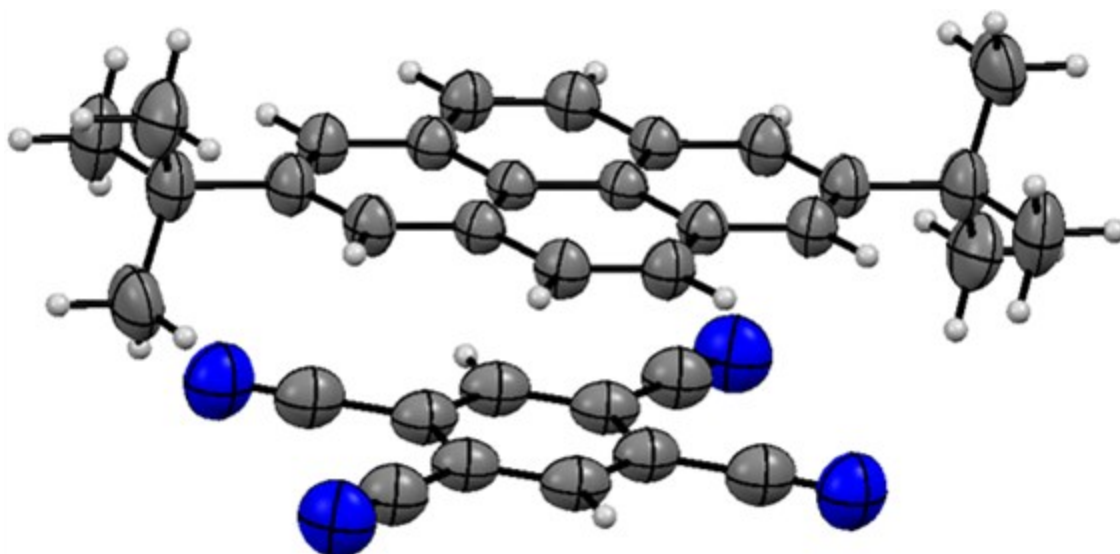


**Figure S4.** ORTEP diagram of cocystal 2.

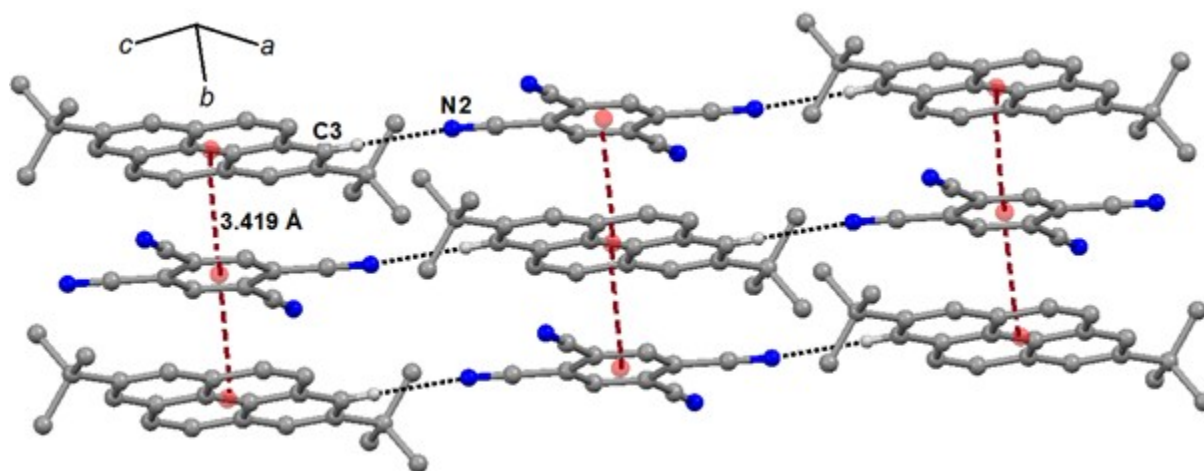


**Figure S5.** Crystal packing of cocrystal **2** is stabilized by face to face  $\pi\cdots\pi$  stacking and C-H $\cdots$ N hydrogen bond.

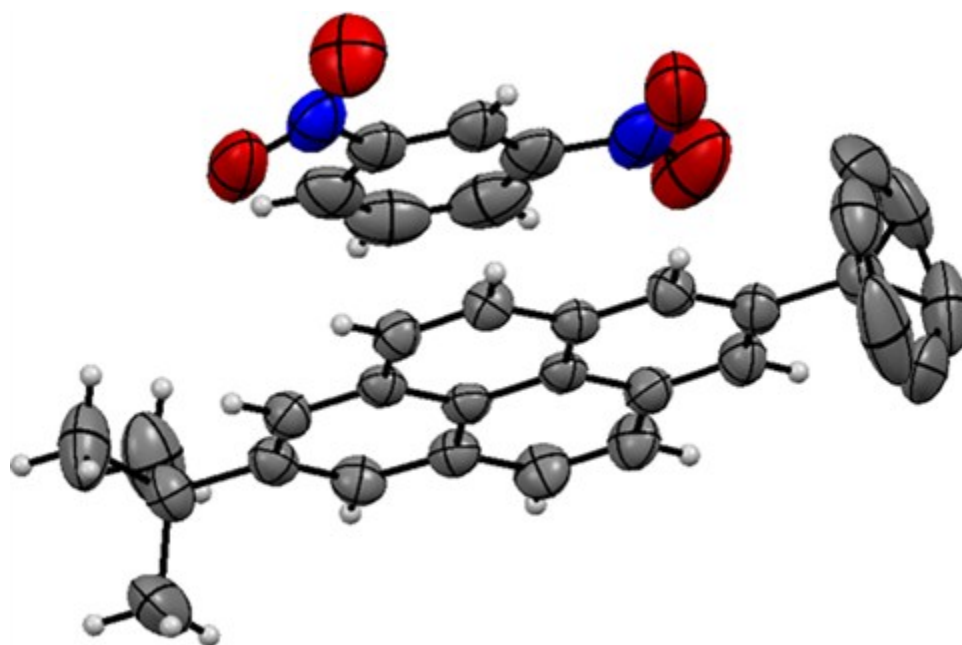


**Figure S6.** ORTEP diagram of cocrystal **3** (hydrogen atoms on disordered *tert*-butyl group are omitted for clarity).

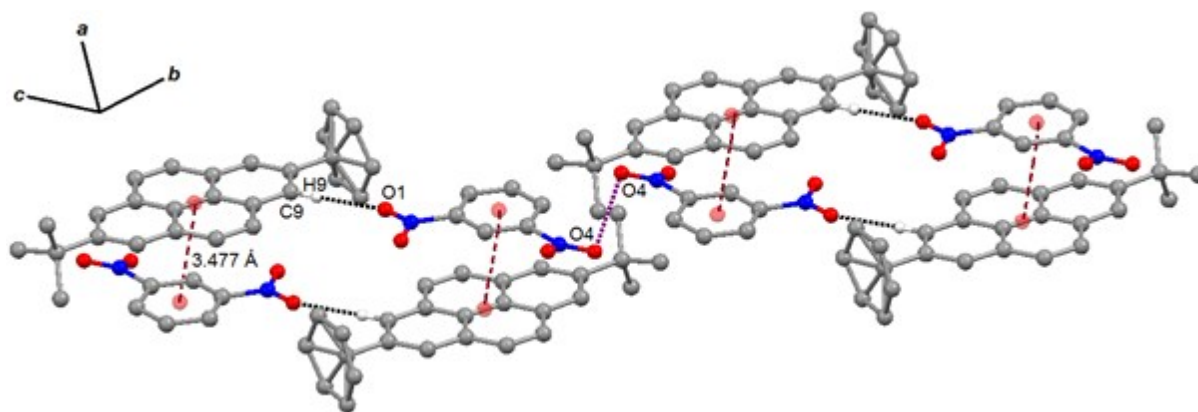


**Figure S7.** Crystal packing of co-crystal **3** is stabilized by face to face  $\pi\cdots\pi$  interaction, weak C–H $\cdots$ O hydrogen bond.

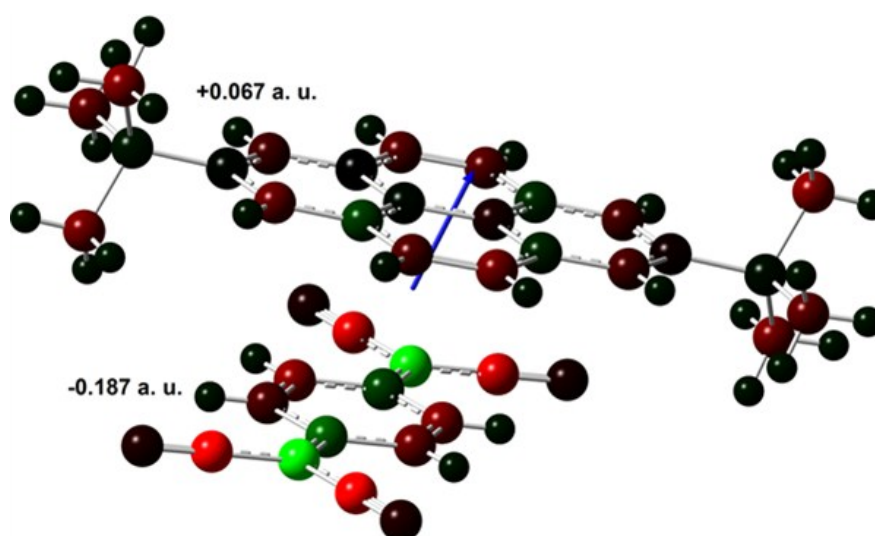


**Figure S8.** Static dipole moment (SDM) of cocrystal **1**, the atoms are coloured according to Mulliken charge on them.

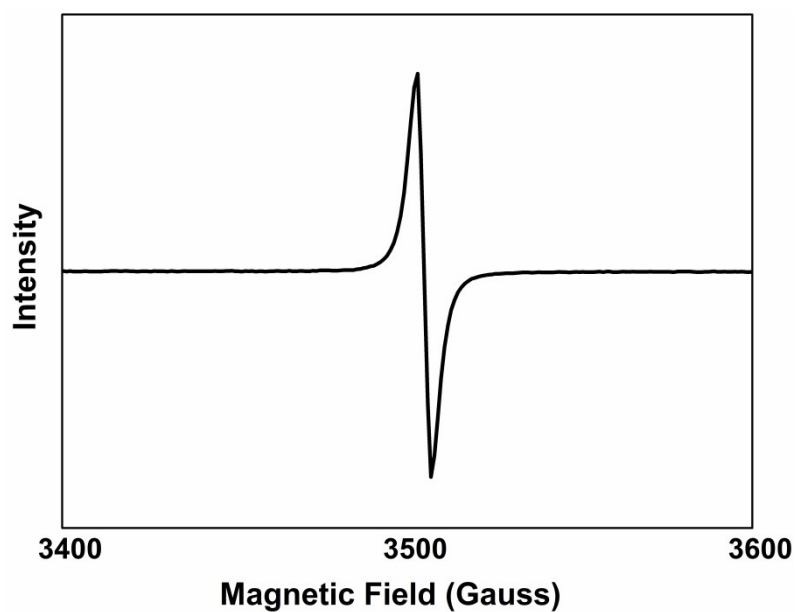


**Figure S9.** EPR spectrum of cocystal **1** shows a strong signal, the strong signal may indicate presence of impurity in TCNQ.

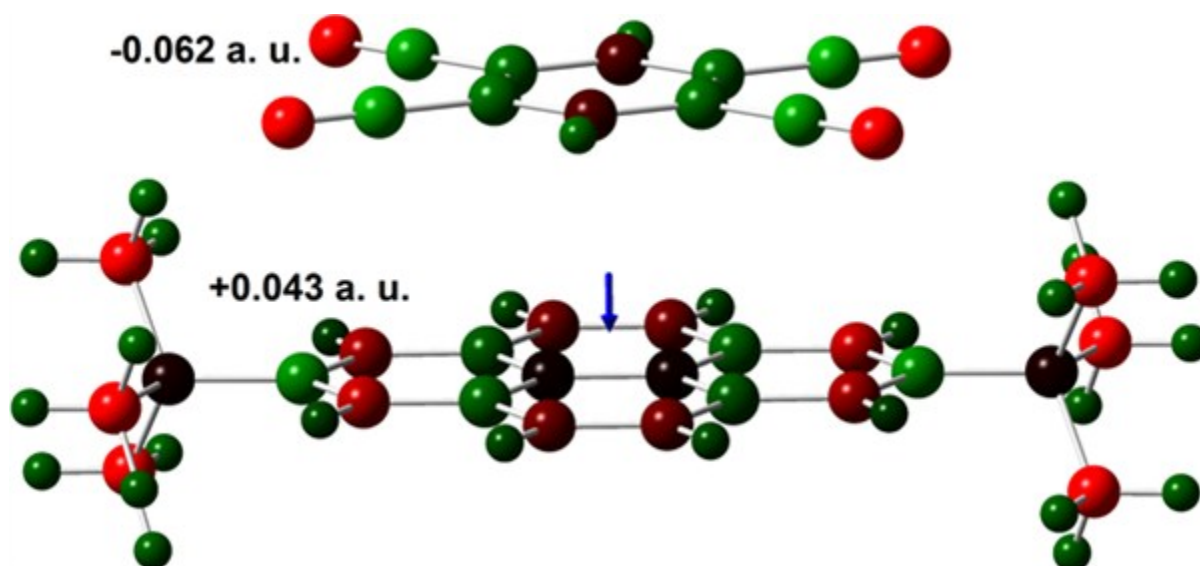


**Figure S10.** Static dipole moment (SDM) of cocystal **2**, the atoms are coloured according to Mulliken charge on them.

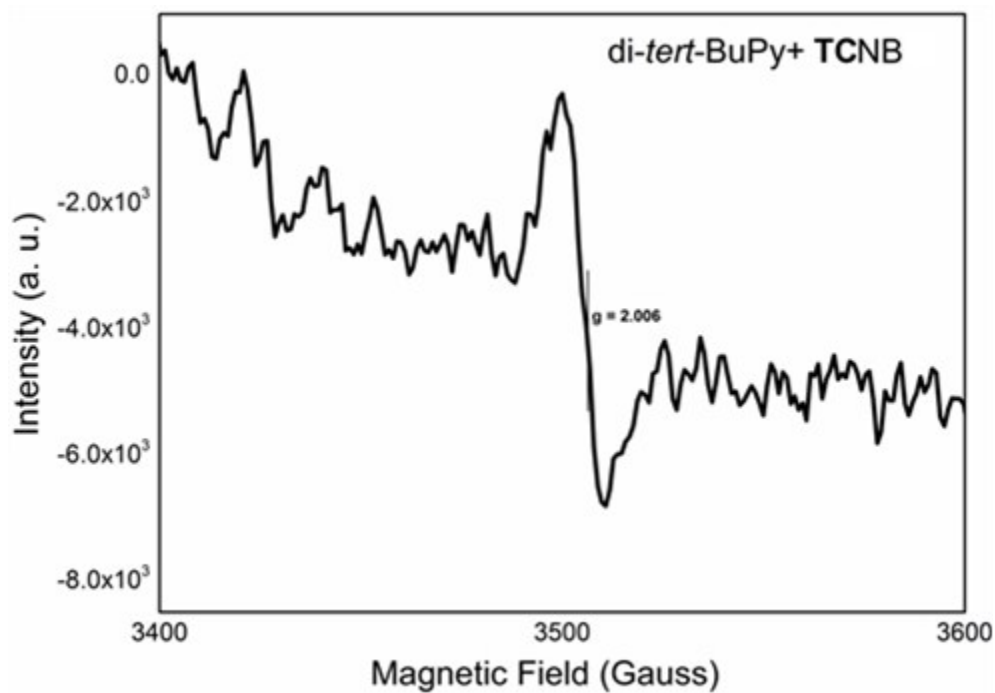


**Figure S11.** EPR spectrum of cocrystal 2 shows a weak signal.

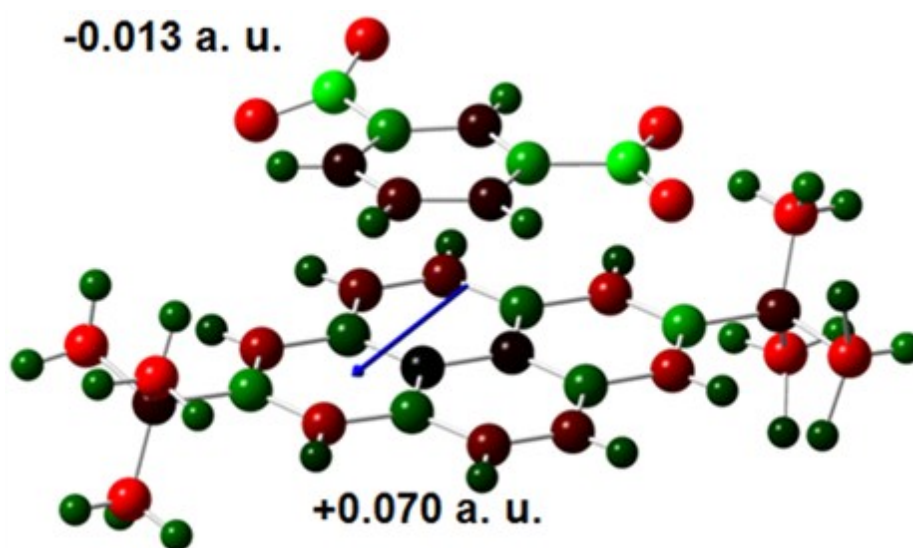


**Figure S12.** Static dipole moment (SDM) of cocrystal 3.

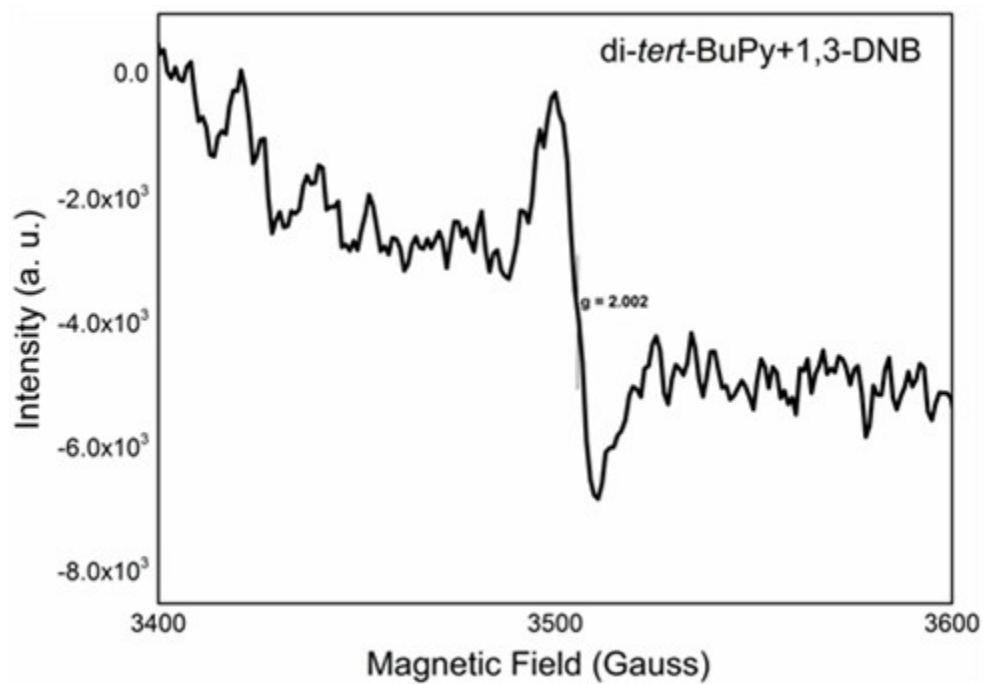


**Figure S13.** EPR spectrum of cocystal 3.

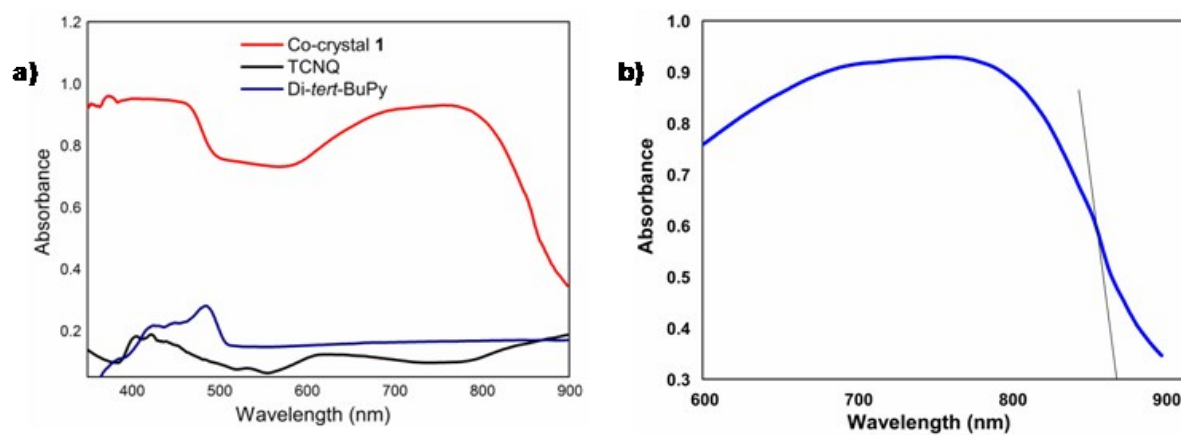


**Figure S14.** (a) UV-Vis spectrum of cocystal 1 in solid state; (b) Application of Kubelka-Munk equation in solid absorption spectrum of cocystal 1.

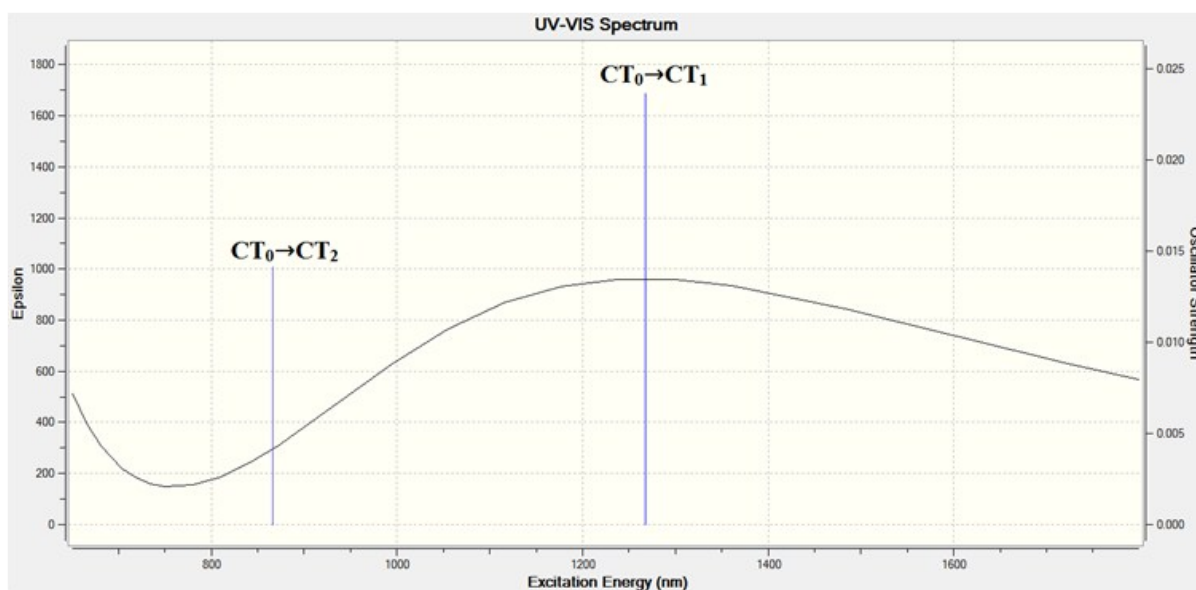


**Figure S15.** Calculated UV-Vis spectrum of cocystal **1** using CAM-B3LYP/6-311G(d,p) level of theory.

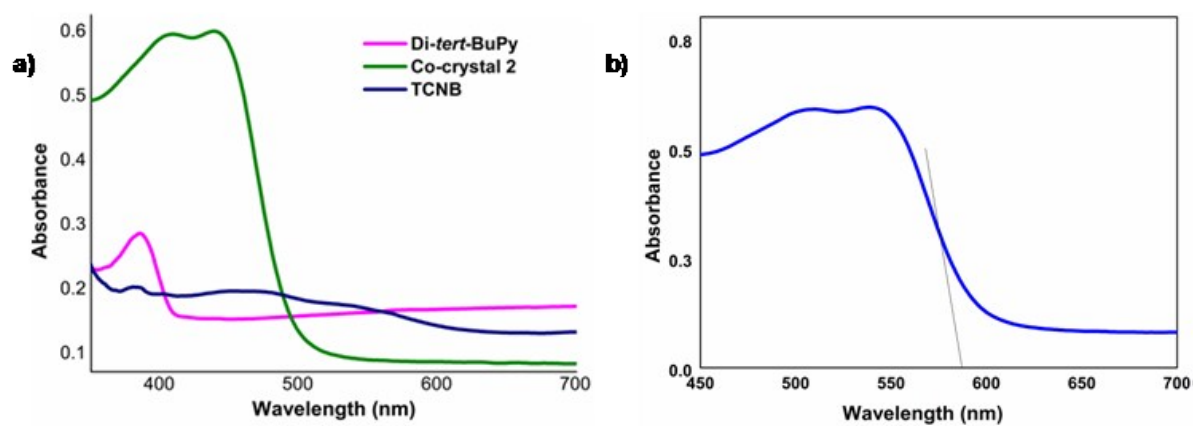


**Figure S16.** a) UV-Vis spectrum of cocystal **2** in solid state; b) Application of Kubelka-Munk equation in solid absorption spectrum of cocystal **2**.

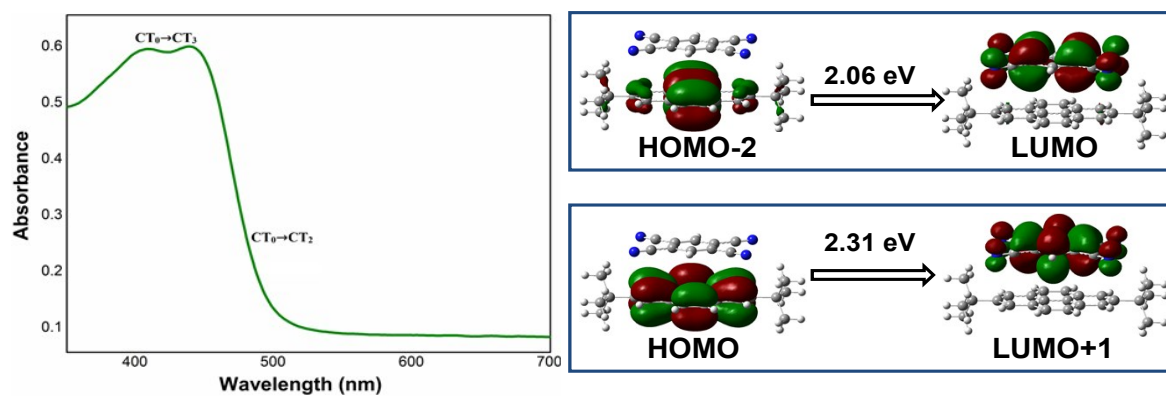


**Figure S17.** Interpretation of absorption spectrum of cocystal 2.

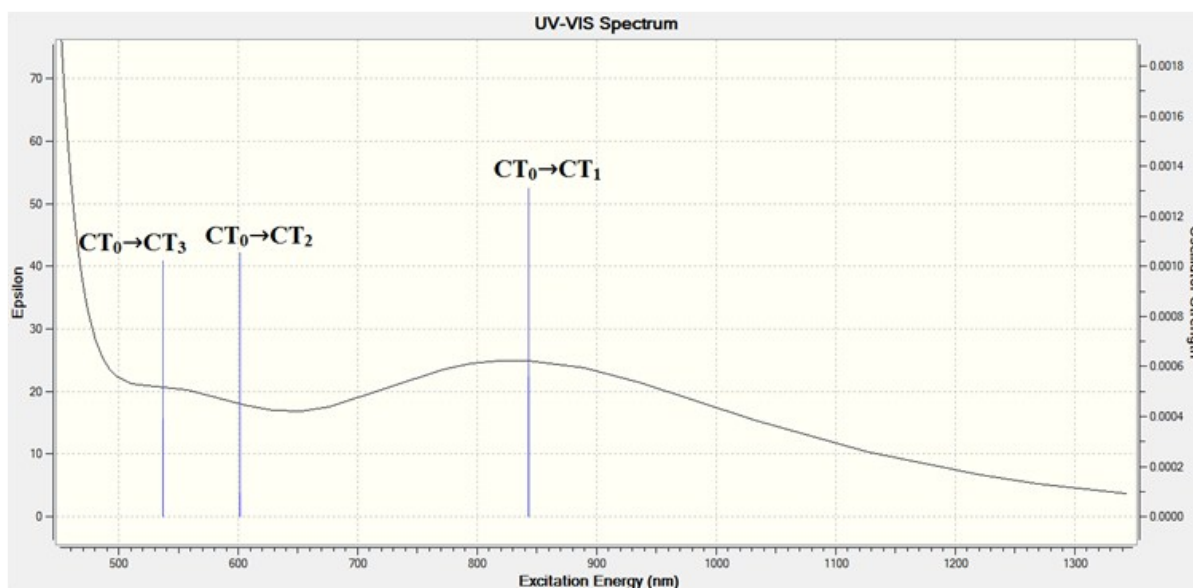


**Figure S18.** Calculated UV-Vis spectrum of cocystal 2 using CAM-B3LYP/6-311G(d,p) level of theory.

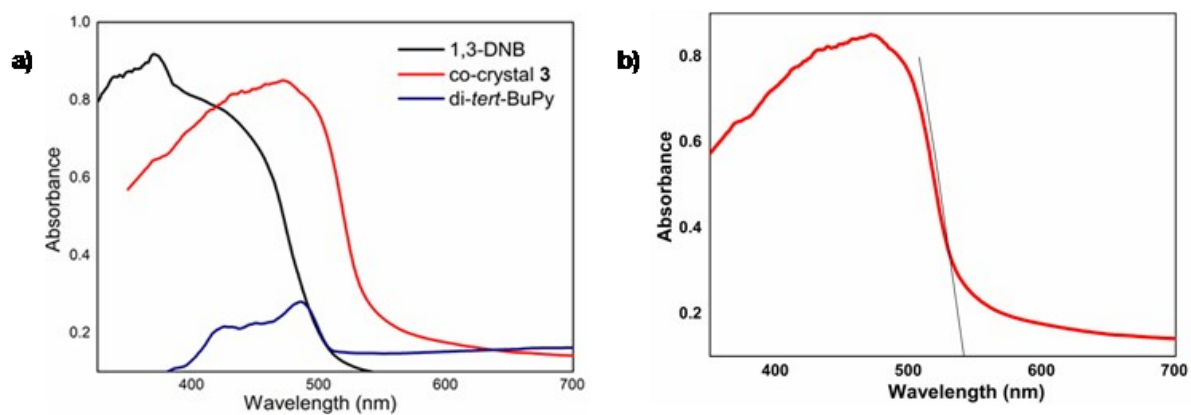


**Figure S19.** a) UV-Vis spectrum of cocystal **3** in solid state; b) Application of Kubelka-Munk equation in solid absorption spectrum of co-crystal **3**.

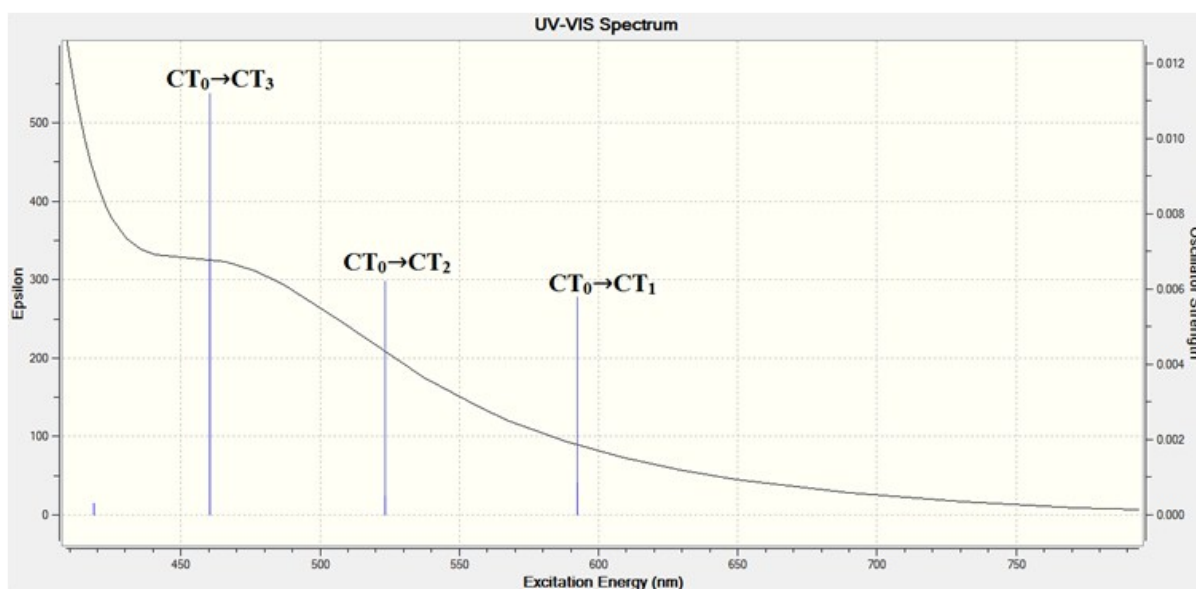


**Figure S20.** Calculated UV-Vis spectrum of cocystal **3** using CAM-B3LYP/6-311G(d,p) level of theory.

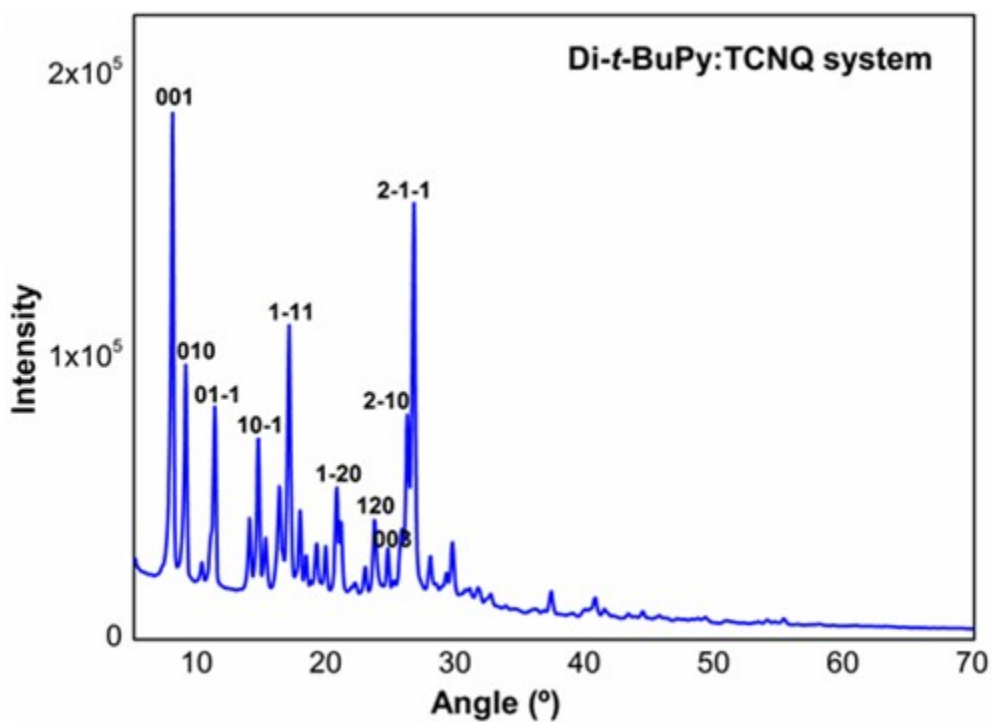


**Figure S21.** PXRD pattern of cocystal **1** high purity of crystalline phase.

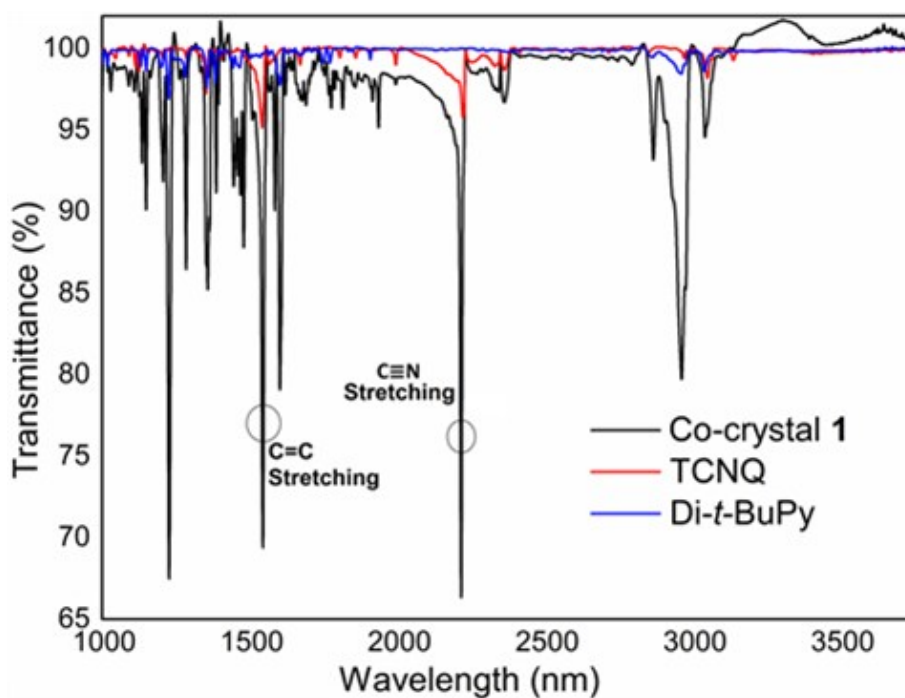


**Figure S22.** IR spectrum of cocystal **1** shows no significant shift of C≡N stretching frequency.

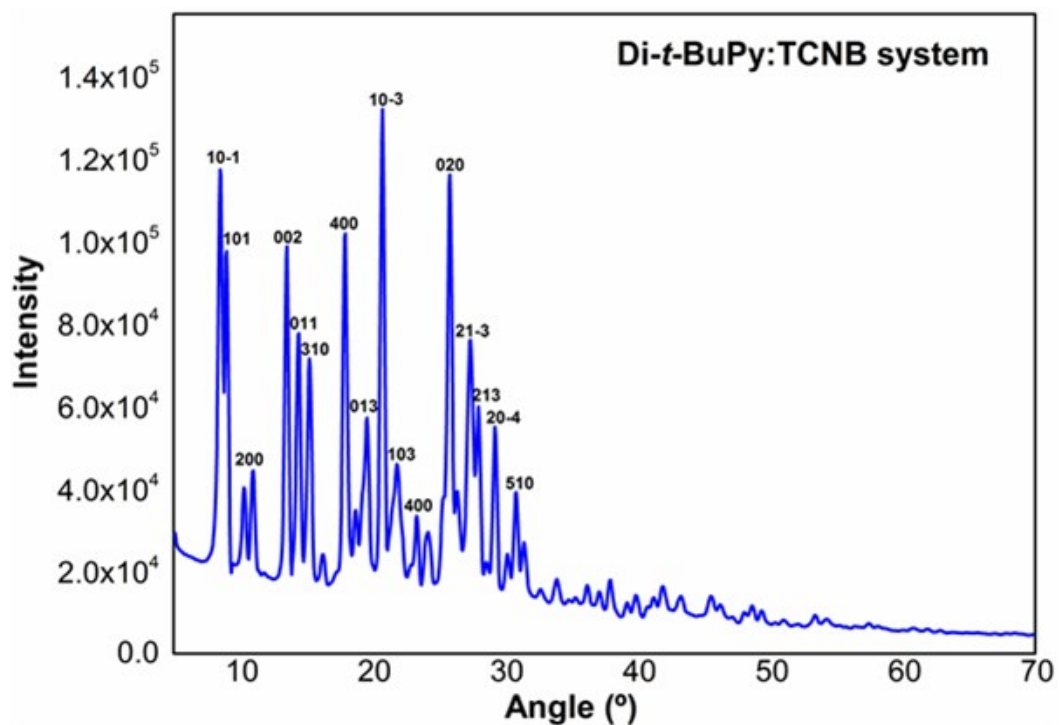


Figure S23. PXRD pattern of cocystal 2 shows high purity of crystalline phase.

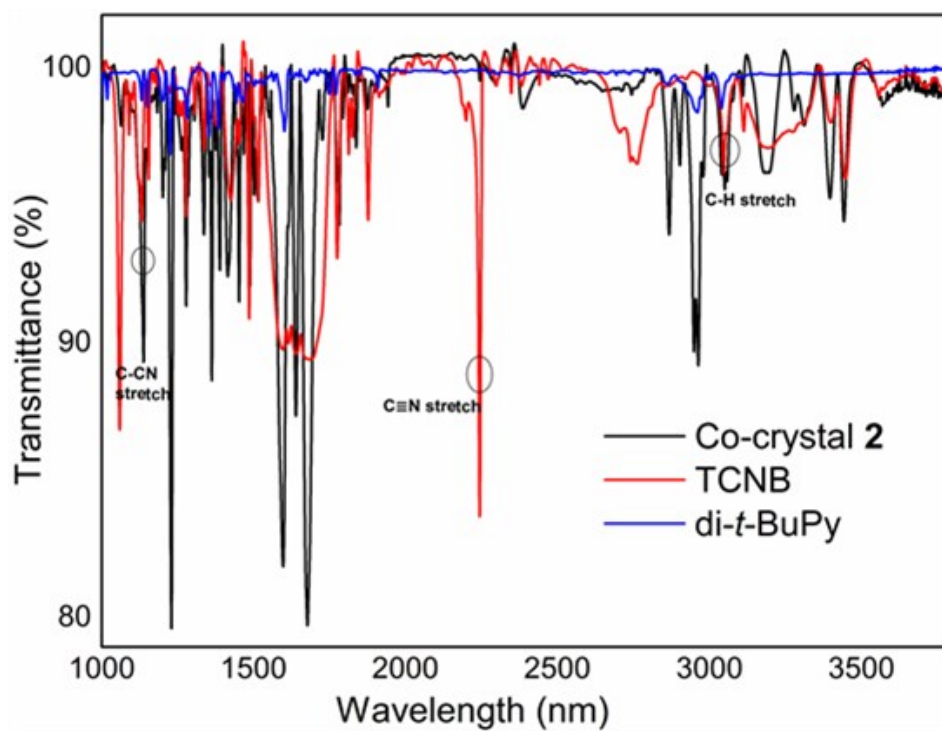


Figure S24. IR spectrum of cocystal 2.

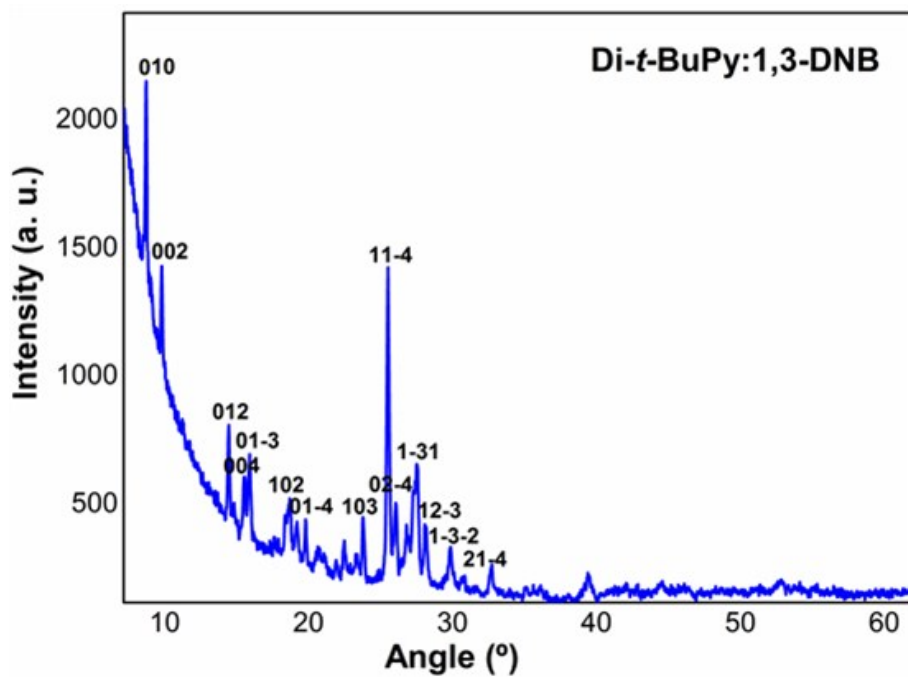


Figure S25. PXRD pattern of cocystal 3 shows high purity of crystalline phase.

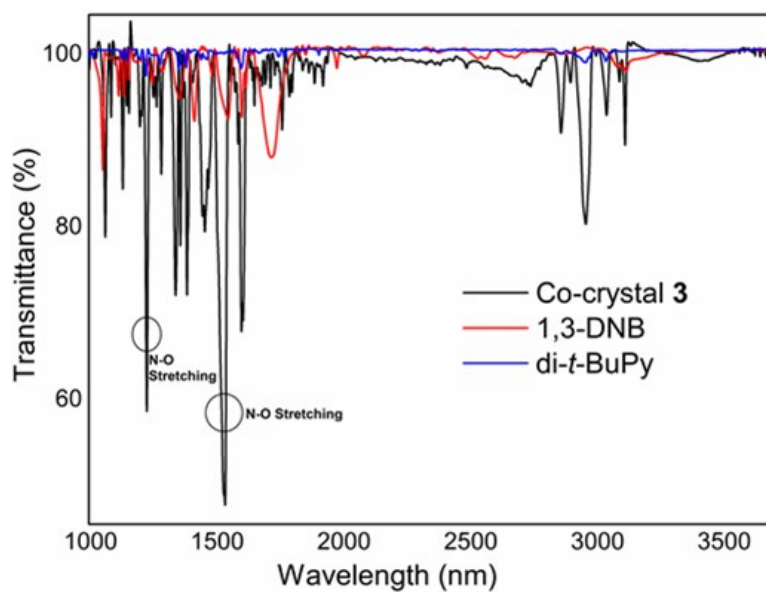
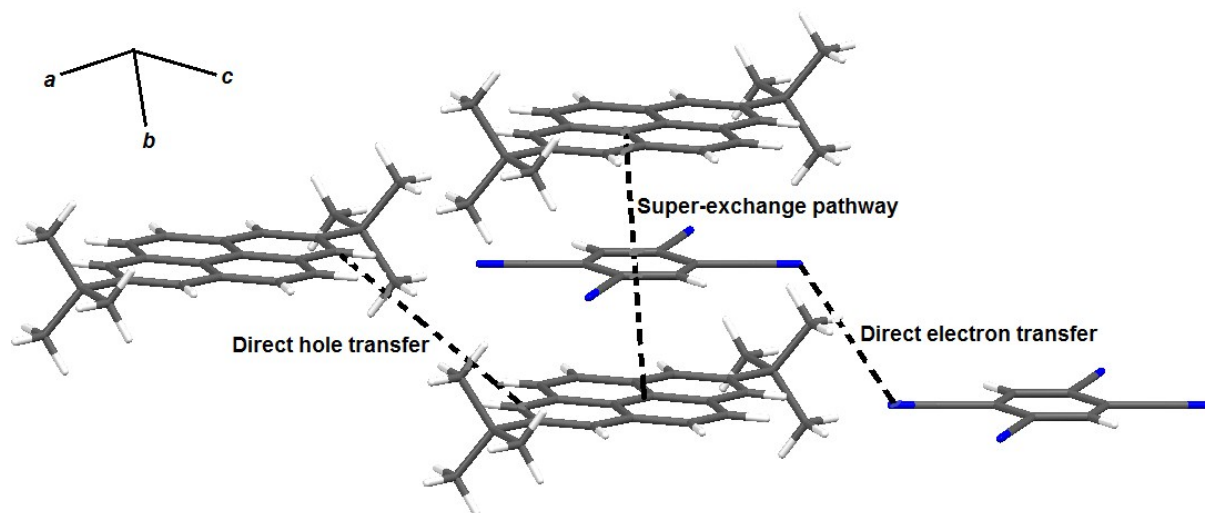
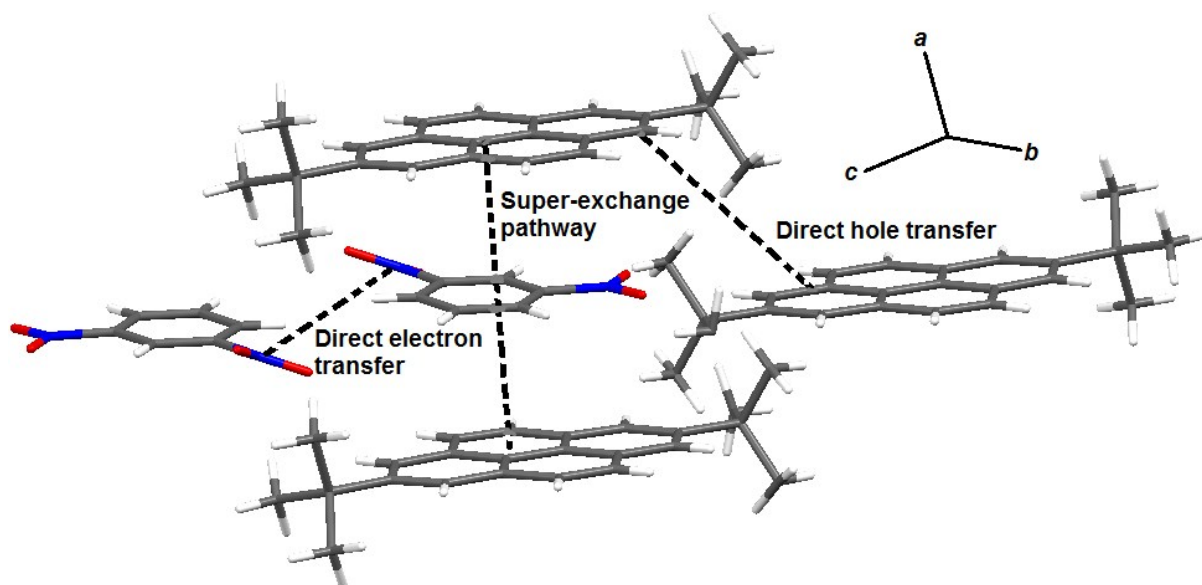


Figure S26. IR spectrum of cocystal 3.



**Figure S27.** Direct and super-exchange electron/ hole carrier pathways in cocrystal 2.



**Figure S28.** Direct and super-exchange electron/ hole carrier pathways in cocrystal 3.

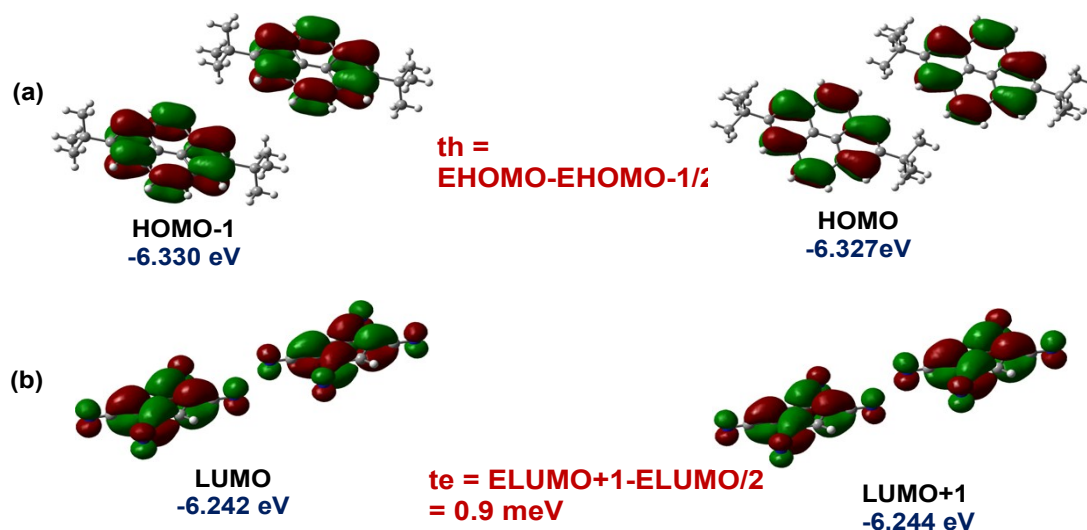


**Figure S29.** Electron and hole transfer integrals by direct charge transfer pathway in cocystal 2, the small values indicate practically no charge transfer via direct path.

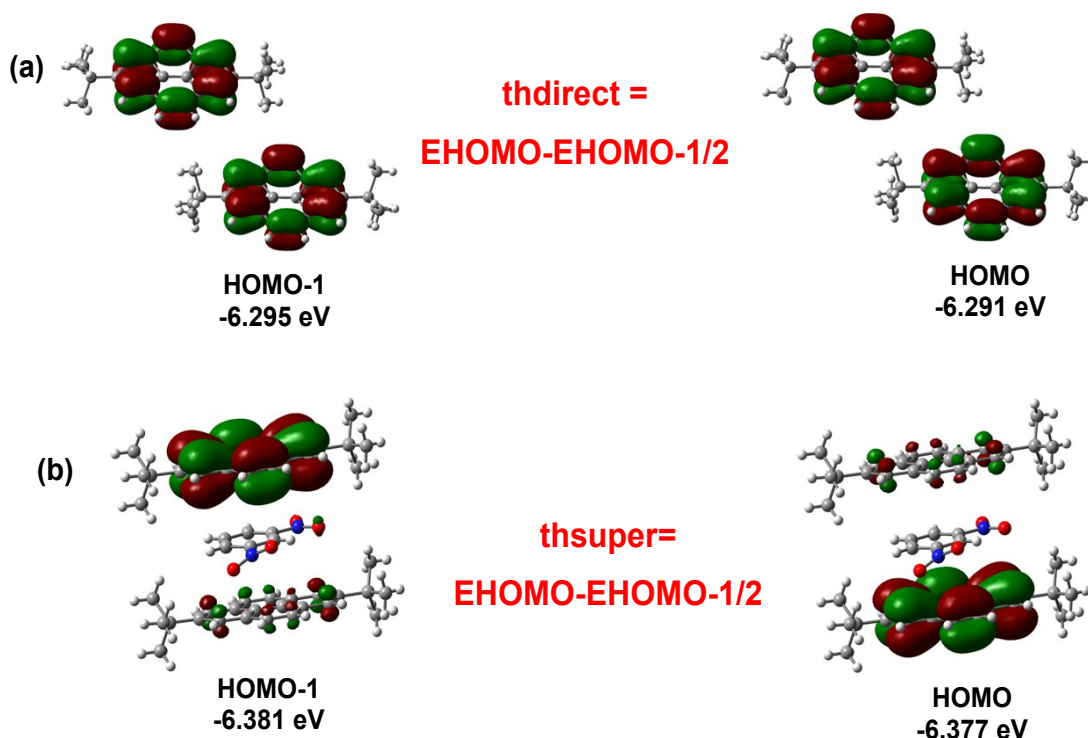


**Figure S30.** Hole transfer integrals for direct and super-exchange pathways in cocystal 3, small values of hole transfer integral indicates comparatively lower degree hole transport.

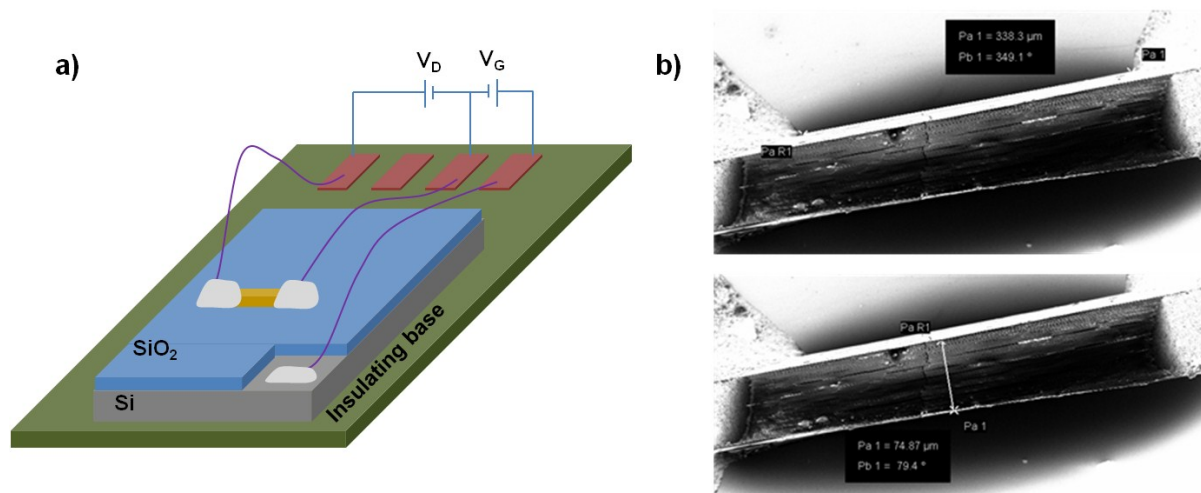


**Figure S31.** (a) Top contact bottom gate device used for measurement; (b) FE-SEM image of cocystal **1** used in SC-OFET.

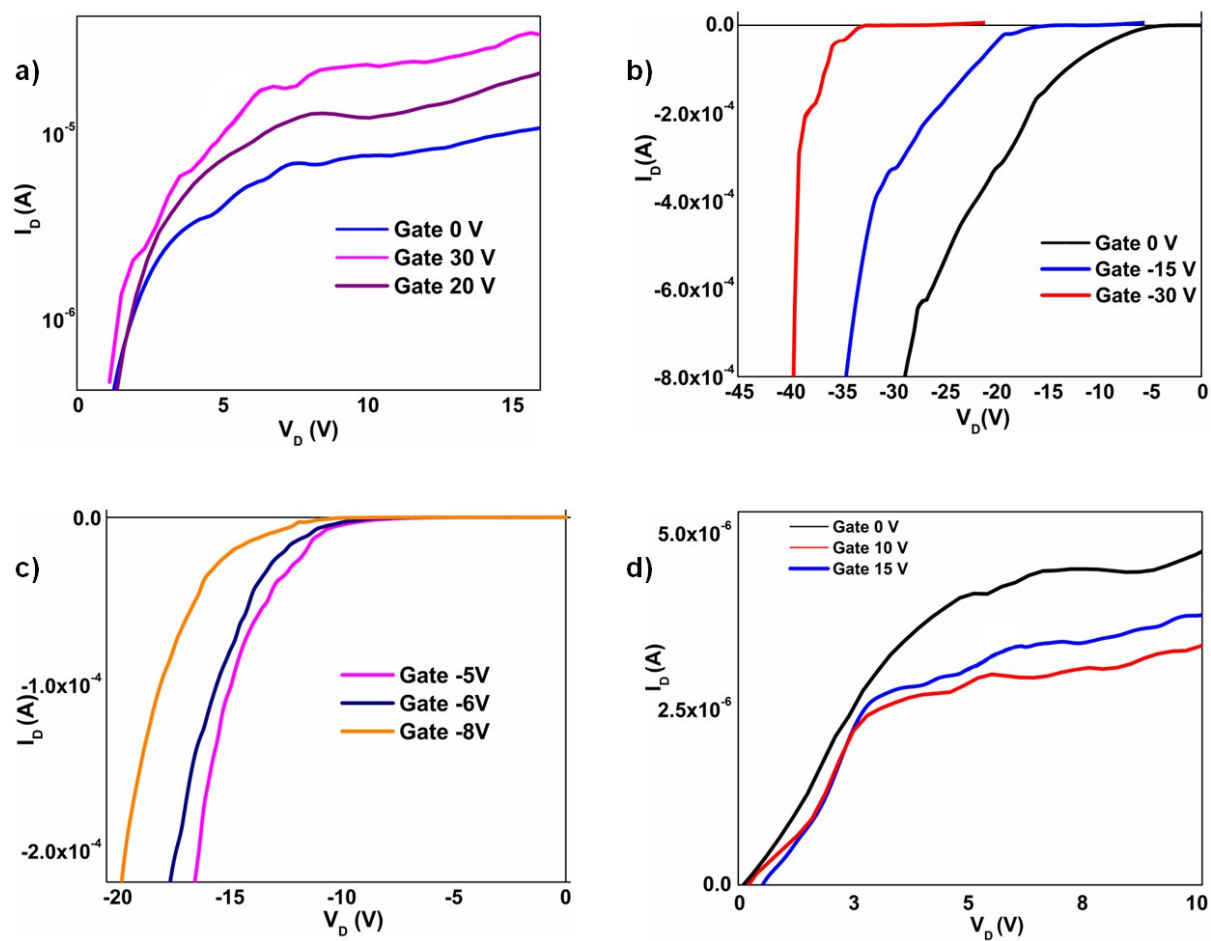


**Figure S34.** (a) Output characteristic at negative drain voltage in cocrystal **1**; (b) Output characteristic at positive drain voltage in cocrystal **1**; (c) Output characteristic at negative drain voltage in cocrystal **2**; (b) Output characteristic at positive drain voltage in cocrystal **3**;  $V_D$ ,  $V_G$  and  $I_D$  denote drain voltage, gate voltage and drain current.

**Table S1.** Intermolecular interactions in cocrystal **1-3**

Cocrystal	Interaction	D...A (in Å)	H...A (in Å)	D-H...A (in °)	Symmetry
<b>1</b>	Cg...Cg	3.496(3)			-x+1, -y+1, -z+1
	C2-H2...N2	3.665(2)	2.76	165	x, y-1, z
<b>2</b>	Cg...Cg	3.419(3)			x, y-1, z
	C3-H3...N3	3.593(3)	2.67	172	x-1/2, y+1/2, z+1/2
<b>3</b>	Cg...Cg	3.477(2)			x, y, z
	C9-H9...O1	3.640(2)	2.72	170	-x+1, -y+1, -z
	O4...O4	2.805(3)			-x+1, -y+1, -z+1

**Table S2.** Electron ( $\mu_e$ ) and hole ( $\mu_h$ ) mobility values ( $\text{cm}^2\text{V}^{-1}\text{s}^{-1}$ ) of cococrystals **1, 2** and **3**

Cocrystal	Electron mobility ( $\mu_e$ )	Hole mobility ( $\mu_h$ )
<b>1</b>	$1.2 \times 10^{-1}$	$1.1 \times 10^{-1}$
<b>2</b>	$9.6 \times 10^{-4}$	Negligible
<b>3</b>	$8 \times 10^{-2}$	$2.2 \times 10^{-4}$